Article

Not peer-reviewed version

Anisotropic Tensile and Compressive Strengths of Al–4wt.%Cu Alloy Powder: Part 1—Effects of Compaction Loads and Heat Treatments

Rodrigo Silva Bonatti , Ausdinir D. Bortolozo , Rodrigo F.G. Baldo , Erik Poloni , Wislei R. Osório *

Posted Date: 5 September 2023

doi: 10.20944/preprints202309.0202.v1

Keywords: aluminum composite; Al–Cu alloys; natural aging; annealing; mechanical properties, environmental aspects

Article

Anisotropic Tensile and Compressive Strengths of Al–4wt.%Cu Alloy Powder: Part 1—Effects of Compaction Loads and Heat Treatments

Rodrigo S. Bonatti [1], Ausdinir D. Bortolozo [1,2], Rodrigo F.G. Baldo [2] , Erik Poloni [3] and Wislei R. Osório [1,2,*]

[1] School of Technology, Campus I, University of Campinas/UNICAMP, 13484-332 Limeira-SP, Brazil; robonatti@yahoo.com.br (R.S.B.); ausdinir@unicamp.br (A.D.B.); rfgbaldo@unicamp.br (R.F.G.B.)
[2] School of Applied Sciences, FCA, Research Group in Manufacturing Advanced Materials (CPMMA), Campus II, University of Campinas/UNICAMP, 13484-350 Limeira-SP, Brazil;
[3] Centre for Advanced Structural Ceramics, Department of Materials, Imperial College London, SW7 2ZA London, United Kingdom.; e.poloni@imperial.ac.uk
* Correspondence: wislei1@unicamp.br

Abstract: Powder metallurgy is a preferred manufacturing method in various industries because it offers design flexibility, material efficiency and a cost-effective production. In this work, we study the effects of different compaction directions on the strength of parts produced by powder metallurgy. Al–4wt.%Cu alloys are used due to their recyclability, and three distinctive compaction pressures are applied, resulting in two sample groups. One group is air-cooled after sintering, while the other is water-quenched and naturally aged (T4 temper). Both the compressive and tensile strengths are measured and analyzed. The study reveals that both heat treatments and compaction directions significantly influence anisotropic strengths. The novelty of this research lies in the use of powders that can be reused from machining, turning, or foundry rejection. By omitting or reducing the melting stage and employing simple powder metallurgy, the cost-effective and environmentally friendly processes are achieved. The planning of compaction load, compaction direction, and heat treatments is found to play a crucial role in determining the final mechanical performance. Notably, this approach aligns with the environmental, social and governance (ESG) practices that have been increasingly adopted by industry.

Keywords: aluminum composite; Al–Cu alloys; natural aging; annealing; mechanical properties; environmental aspects

1. Introduction

In powder metallurgy, compaction is an essential step performed before sintering a green body. It is crucial to accurately determine the compaction loads and density distributions in the final product, and the parameters required for this process depend on the desired or planned application. Factors such as particle size and shape, mechanical features, and particle-surface properties significantly influence the resulting preform [1]. Furthermore, the geometry and surface characteristics of the tools used in compaction, along with the control of applied loads, play a vital role in determining the final soundness and properties of the product [2]. Numerous models [3-6] have been proposed to explain the compaction behavior of powders, but accurately predicting the mechanical properties remains challenging. Previous studies have shown that the strength of a compact depends on the compaction mode employed [5-7]. Generally, the tensile strength perpendicular to the compaction direction is higher than that along the compaction direction.

Extensive literature, including studies on strength anisotropy in distinct materials during cold compaction, pressing, and after sintering, has been reviewed [7]. The results show that both ductile and brittle powders exhibit strength anisotropy, which is influenced by density. In the case of ductile

 doi:10.20944/preprints202309.0202.v1

powders, the highest strength was observed in the transverse direction due to crack deflection resulting from increased particle overlap and flattening. For brittle powders, it was proposed that particle fragmentation along the compaction direction weakens the strength in the transverse direction [7]. Previous work also presented models that successfully explain the mechanisms related to strength anisotropy [2; 8-9] Loidlt et al. have used model using multi-particle finite element method [2] to predict the anisotropic elastic and plastic properties. Cao et al [8] have reported the anisotropy in tensile mechanical properties of bulk Al samples fabricated by spark plasma sintering. Xu et al [9] investigated the anisotropic mechanical behavior of phyllite material. However, the impact of heat treatments on the microstructure of compacted powders has not been thoroughly investigated in the past decades. Although different heat treatments are widely employed in industry and significant improvements in the properties of 2xxx (Al–Cu) casting alloys and composites have been reported [10-15], there is a clear lack of systematic studies supporting these findings.

In this work, we used an alloy powder to investigate the impact of compaction pressure, strength anisotropy, and heat treatment on the microstructure and mechanical properties of sintered parts. First, we compacted powders in the transverse and longitudinal directions at different pressures. Next, the samples were densified using sintering parameters previously optimized [16-19]. In the final stage of the sintering cycle, the samples were either air-cooled or subjected to water-quenching, followed by natural aging. Finally, both the compressive and tensile strengths were characterized. A particular contribution of this work lies in the use of Al–4wt.%Cu (Al–4Cu) alloys, which can be recycled from conventional machining, drilling, and turning processes, or taken from rejection volumes in foundries [16-20]. The recyclability of these alloys helps reduce the overall costs associated to conventional processing routes based on atomization and electrolytic methods. While the use of ball milling to adjust particle size distribution still impacts the use of recycled powders, this work represents a step forward in developing processing routes that address the need for both environmental friendliness and cost-effectiveness in alloy production. As environmental, social and governance (ESG) considerations have gained increased significance within investors, consumers, and stakeholders, scientific research is expected to play a key role in enabling new practices within industries [21].

2. Materials and Methods

2.1. Initial Materials, Powder Production and Compaction

The samples of an as-cast Al–4wt.%Cu alloy were generated using a permanent steel mold (low-carbon, SAE 10145). This alloy composition was chosen due to its extensive usage in aerospace and automotive applications [10, 15-18]. Conventional gravity solidification was employed, and the alloy was poured into the steel mold in flowing argon (~2 L/min). The Al–4Cu alloy was elaborated by using commercial pure Al (99.8 wt.% Al, Alux and Albras, Brazil). The Al had impurities such as 0.11 wt.% Fe, 0.06 wt.% Zn, 0.02 wt.% Mn, and less than 0.009 wt.% Cu, with other impurities below 0.001 wt.%. Electrolytic Cu (99.89 wt.% Cu) was added to achieve the desired alloy composition.

The initial powders are obtained by using a drilling of the as-cast ingots. The cylindrical as-cast Al–4Cu alloy ingots with an outer diameter of 50 mm were drilled to obtain flake-shaped powder particles. To prevent the presence of oxides (from casting procedure) in the drilled powder, the surface of the ingots were initially ground to remove the oxide film. After, drilling is carried out and obtained powder portion is immediately compacted (no storage is applied). It is important to notice that we did not use sieves, which eliminates the need for time-consuming sieving stages. Previous studies have shown that this approach offers a favorable balance between sieving time, particle morphology, and achieved densification level [18-20].

The produced powders were compacted using a hydraulic press and two different tempered dies out of VC-131 steel with a hardness of 60 HRC (Figure 1a,c). Transverse specimens (32x5x2 mm) are produced by applying the compaction load in a direction perpendicular to that of the mechanical characterization (red arrows, Figure 1b). When employing a double-action compaction die (Figure 1c), the cylindrical (ϕ6x35 mm) specimens are produced by compacting along the specimen's

Preprints (www.preprints.org) | NOT PEER-REVIEWED | Posted: 5 September 2023 doi:10.20944/preprints202309.0202.v1

symmetry axis (Figure 1d). To characterize the compressive strength of transverse samples, sections of the sample depicted in Figure 1(b) are used, and compressive pressures (blue arrows) are applied perpendicular to the compaction direction (red arrows). When cylindrical specimens are subjected to a transverse load (Figure 1(d)), the Brazilian indirect tensile test is used. The transverse and longitudinal specimens are produced using 1 and 3 g of the Al–4Cu alloy powder, respectively. The compaction pressures of 300, 400, and 600 MPa were used to produce for all specimens and the experimental procedure was repeated in triplicate to ensure the reproducibility of the results. Although different shapes are utilized (flatted or transversal and cylindrical or longitudinal), it is important to remark that no deleterious effects were observed in the experimental results. With the present experimentation, it is verified that the "flatted" specimens have same results when performed in compressive and tensile tests, as shown in Figure 1(e). This is forwardly discussed in section 3.2. It is expected since a same compaction direction is provided and same mechanical direction is carried out. A more detailed discussion concern to matter is provided at section 3.3.2, particularly in Figure 9(a) and 9 (b).

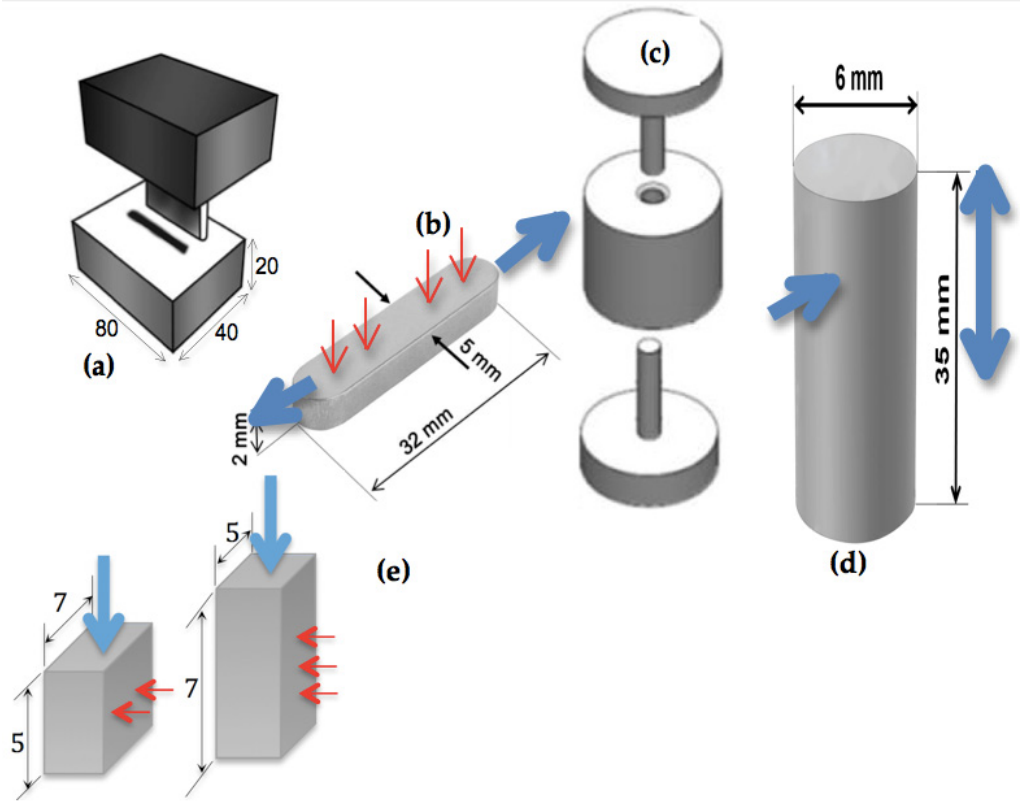

Figure 1. Schematic representation of: **(a)** The compacting die used to produce **(b)** transverse samples; The **(c)** double-action compaction die used to produce **(d)** cylindrical longitudinal samples; **(e)** The two perpendicular directions used to characterize the mechanical properties of transverse samples. The red arrows indicate compacting directions, and the blue arrows indicate tensile and compression directions. It is remarked that gauge lengths are 15 (±0.1) mm and 30 (±0.1) mm for the transversal and longitudinal samples, respectively.

2.2. Densification Measurements and Heat Treatments

The densification of both the green and sintered samples was calculated using Archimedes' principle, according to Equations #1 and #2 (ASTM B692/17).

$$Td = (dAl \times wt.\%Al) + (dCu \times wt.\%Cu)/100 \quad (1)$$

$$D = ((Ts - Ed)/Td) \times 100 \quad (2)$$

Preprints (www.preprints.org) | NOT PEER-REVIEWED | Posted: 5 September 2023 doi:10.20944/preprints202309.0202.v1

Where Td is theoretical density based on law of mixtures, dAl and dCu are aluminum and copper densities (g/cm³), wt.%Al and wt.% Cu are Al and Cu weight percentages, and Ed means the experimental density used to calculate the densification level (D).

When pure Al and Cu densities were used to determine the theoretical density, this constitutes a simplification from the metallurgical point of view. By using Scheil's equation, an Al-4wt%Cu alloy has eutectic fraction (fe) of about 7.84%, when solidification in non-equilibrium condition is considered [22]. From this "fe" percentage, an amount of 50% is constituted by Al lamellae and other 50% are Cu. Based on this, from the metallurgical point of view, the Al-4Cu density is determined with 92.16% (Al-rich phases) summed with eutectic density (ρfe). This is calculated by considering cooperative Al-rich phases and Cu phases, i.e. 3.92% of Al and 3.92% of Cu, which constitutes 7.84% of the eutectic fraction in typical lamellae morphology. This results in a density of 2.945 g/cm³, while a density of 2.950 g/cm³ is calculated when pure Al and Cu (96 and 4%) are used. No substantial differences are verified. Al-rich phase at lamellar structure contains of about 0.68%Cu (determined by Scheil's equation), which was neglected when 2.945 g/cm³ was determined. When the volume fractions of each phase (Al and Al_2Cu) are determined based on the integrated areas and total areas of all phases [23] obtained from XRD patterns, the percentages of phases corresponding with Al_2Cu and Al are approximately 10.97 and 89.03%, respectively. By using two distinct Al_2Cu densities reported in literature, i.e. 4.53 g/cm³ [24] and 4.35 g/cm³ [25], the resulting densities are of about 2.901 and 2.884 g/cm³, respectively. These representing more slight differences from that theoretical value. These metallurgical assertions are only mentioned as an information purposes. Depending on the alloy used, the calculation of densities using the law of mixing can lead to more significant differences, if the microstructural formation is not properly interpreted.

The initial powders are obtained from Al4Cu casting alloy ingots, an as-cast microstructural array is expected. Therefore, a simple sintering process is adopted, applying a heating rate of approximately 10 °C/min and maintaining a plateau at 540 °C for 1 hour. The time and temperature parameters for sintering are selected based on economic considerations and previous results [16-19]. Additionally, the chosen sintering temperature is lower than eutectic temperature (548 °C), ensuring no liquid portions are formed. The green samples are placed in alumina containers, as shown in Figure 2a, and placed inside a muffle-type furnace under argon (~5 L/min of argon flow).

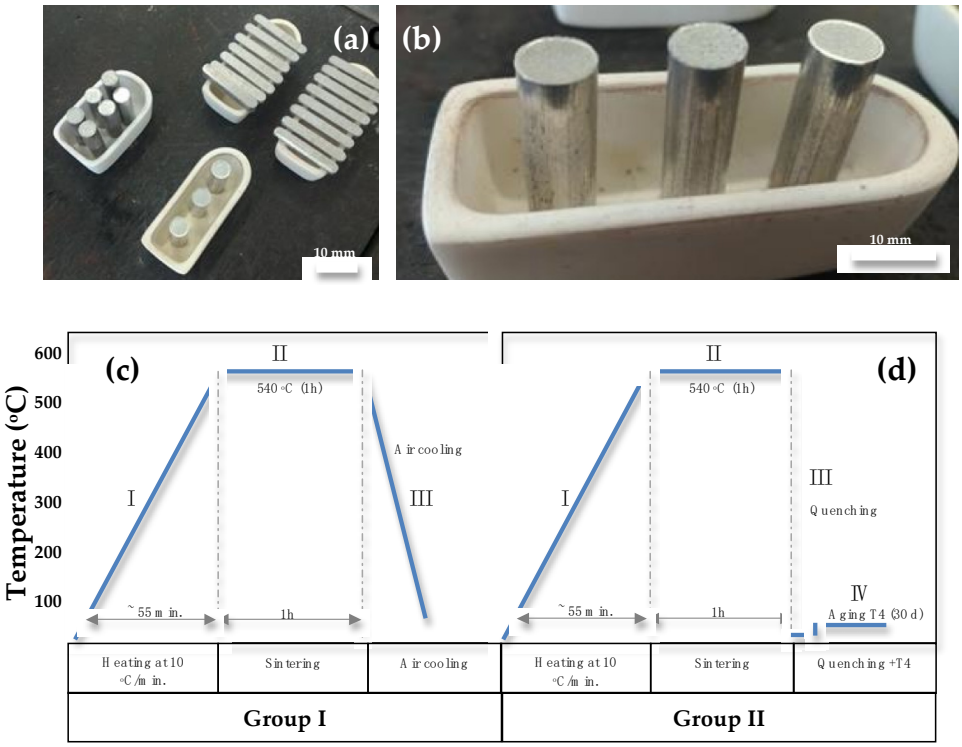

Figure 2. (a) Compacted (green) samples disposed inside **(b)** alumina recipients to sintering; and representation of **(c)** the heating and sintering of samples from group I, and **(d)** group II.

 doi:10.20944/preprints202309.0202.v1

Two groups of compacted Al–4Cu samples are prepared. One group undergoes the aforementioned sintering process followed by air-cooling, similar to annealing. After sintering, the other group of sintered samples is immediately water quenched (at 27 ±2 °C) and naturally aged for 30 days, corresponding to a typical T4 treatment [10-12; 16; 19]. Triplicate samples are used for each group to ensure reproducibility. A schematic representation of the sintering process and subsequent heat treatments is shown in Figure 2b. A summary of the temperatures and times for the different heat treatments was recently reported [15].

Following sintering and heat treatment, the densification level is determined by comparing the theoretical and experimental densities. The green densification is also taken into account for comparison, as previously reported [18]. Triplicate results are used for reproducibility, and average values are considered.

2.3. Mechanical Properties and Microstructural Characterization

To determine the resulting mechanical properties of the sintered and treated samples with different compactions (i.e., transverse and longitudinal), both tensile and compressive tests are conducted following the both MPIF Standards (Metal Powder Industries Federation) #10 and #41, which are similar to ASTM E8M/E9M. Considering the tensile test specimens, it is remarked that gauge lengths are 15 (±0.1) mm and 30 (±0.1) mm for the transversal and longitudinal samples, respectively are considered. The tests are performed at a crosshead speed of 0.25 mm/min, corresponding to a strain rate of approximately 2×10^{-4} s^{-1}, at a temperature of 24 (±2) °C. An electro-hydraulic servo machine (Equilam® model WDW-100E, Time Group Inc., China) is used for the testing. For the samples produced using die compaction (Figure 1(a)), one group is positioned in the machine in the transverse direction. This same group is also tested in a second direction, which is perpendicular or transverse to the compaction direction. When the samples undergo compressive testing in the same direction as the tensile and compressive directions, they are referred to as longitudinal samples.

On the other hand, when both the compressive and tensile tests are carried out in the transverse direction to the compaction direction, the samples are referred to as transverse samples. Although cylindrical and prismatic specimens were used to conduct the mechanical tests, some previous tests have revealed that no deleterious effect in mechanical tendency (behavior) is observed. Based on this, the distinctive specimens' shape was used to guarantee the different compaction direction performed.To characterize the initial powder particles and the resulting microstructure, a scanning electron microscope (SEM), TESCAN® model VEGA3 (Brno, Czech Republic), equipped with an energy-dispersive X-ray (EDX) detector, was used. Additionally, a PANalytical® XPert diffractometer (X'Pert model), Malvern, Worcestershire, U.K., is utilized to determine the structure phases of the examined particles and sintered/treated samples. The diffractometer operates at a voltage of 40 kV and a current of 30 mA, using Cu Kα radiation with a wavelength of 0.15406 nm.

3. Results and Discussion

3.1. Initial Powders and Anisotropic Effect on Densification

Typical SEM images of the as-cast Al–Cu alloy powder particles are shown in Figure 3(a), (b), and (c). The particles are arranged on a conductive carbon adhesive tape inside the microscope chamber. Particle sizes are measured considering both length and width. Due to the reasonable ductile characteristics of the obtained powder, some particles appear more spheroidal, while a majority trend towards flaked or flattened powders is observed. This is a result of the drilling process, as previously reported [16; 18-19].

Preprints (www.preprints.org) | NOT PEER-REVIEWED | Posted: 5 September 2023 doi:10.20944/preprints202309.0202.v1

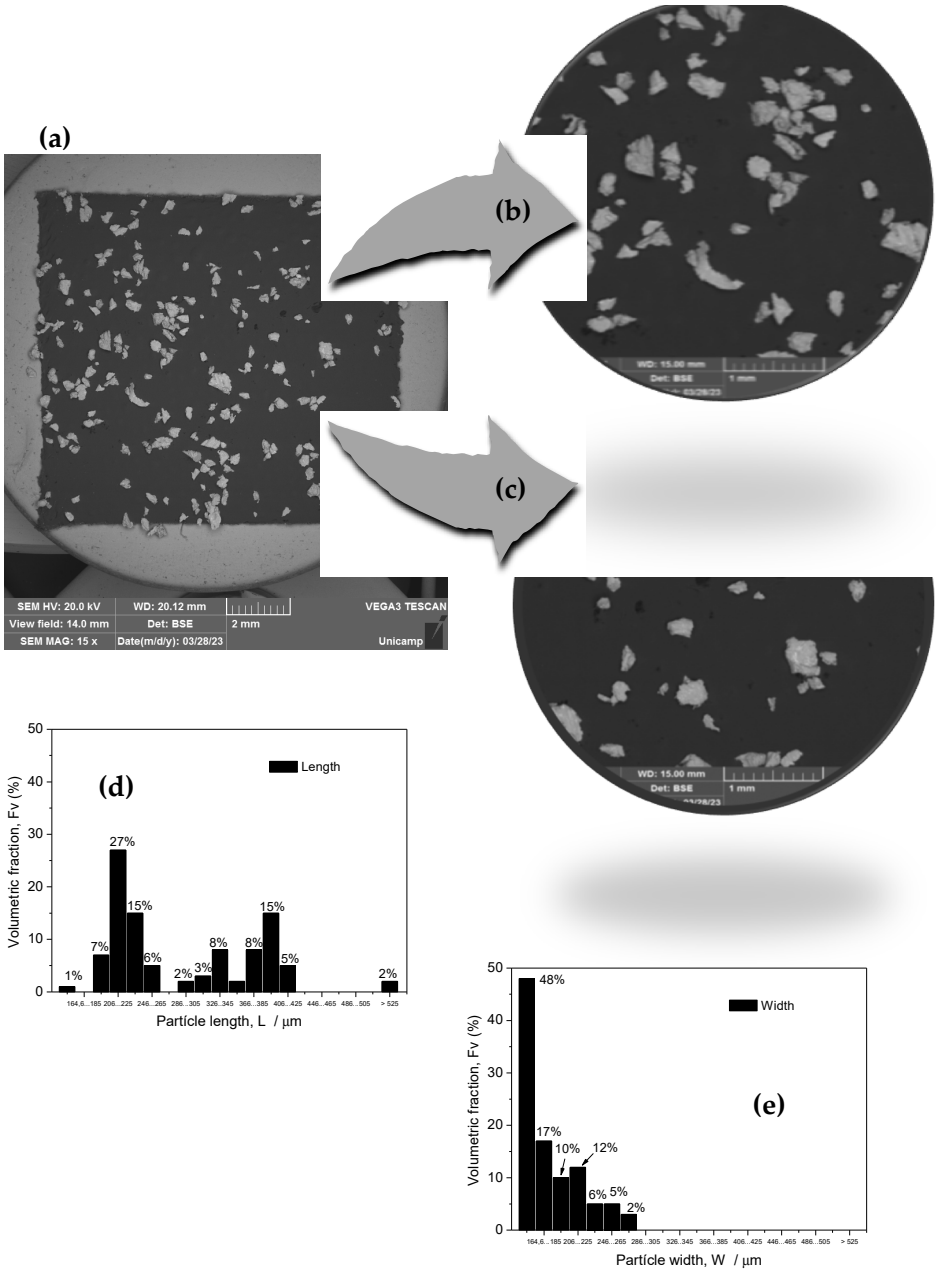

Figure 3. (a) Typical powder particles of the as-cast Al–4Cu alloy inside the chamber of microscope displaced on conductive carbon adhesive, **(b)** and **(c)** distinct regions representing power particles, and **(d)** and **(e)** showing volume fractions of both length and width of the particles examined.

The distributions of particle sizes in terms of length and width are reasonably distinctive. The flattened morphology is characterized by a length that is approximately twice the width, with average values of 290 µm and ~160 µm, respectively. It is also noted that a bimodal distribution for the length of particles is observed, which has also been observed by Satizabal et al [16] and Bonatti et al [18] when compacting ductile particles. It is worth mentioning that no significant modification in morphology and powder size distribution is observed when analyzing groups I and II.

Figure 4(a) shows the resulting compressibility curves, or relative density, for both the green and sintered Al–4Cu alloy samples using three different compaction pressures. Figure 4(b) depicts the same data fitted using Equation #1 against the square root of the compaction pressure, as previously reported [20; 27-28]. This analysis is conducted for the transverse samples. The data are also fitted using the Panelli and Ambrosio Filho equation, which has been reported by Fogagnolo et al [20].

Preprints (www.preprints.org) | NOT PEER-REVIEWED | Posted: 5 September 2023 doi:10.20944/preprints202309.0202.v1

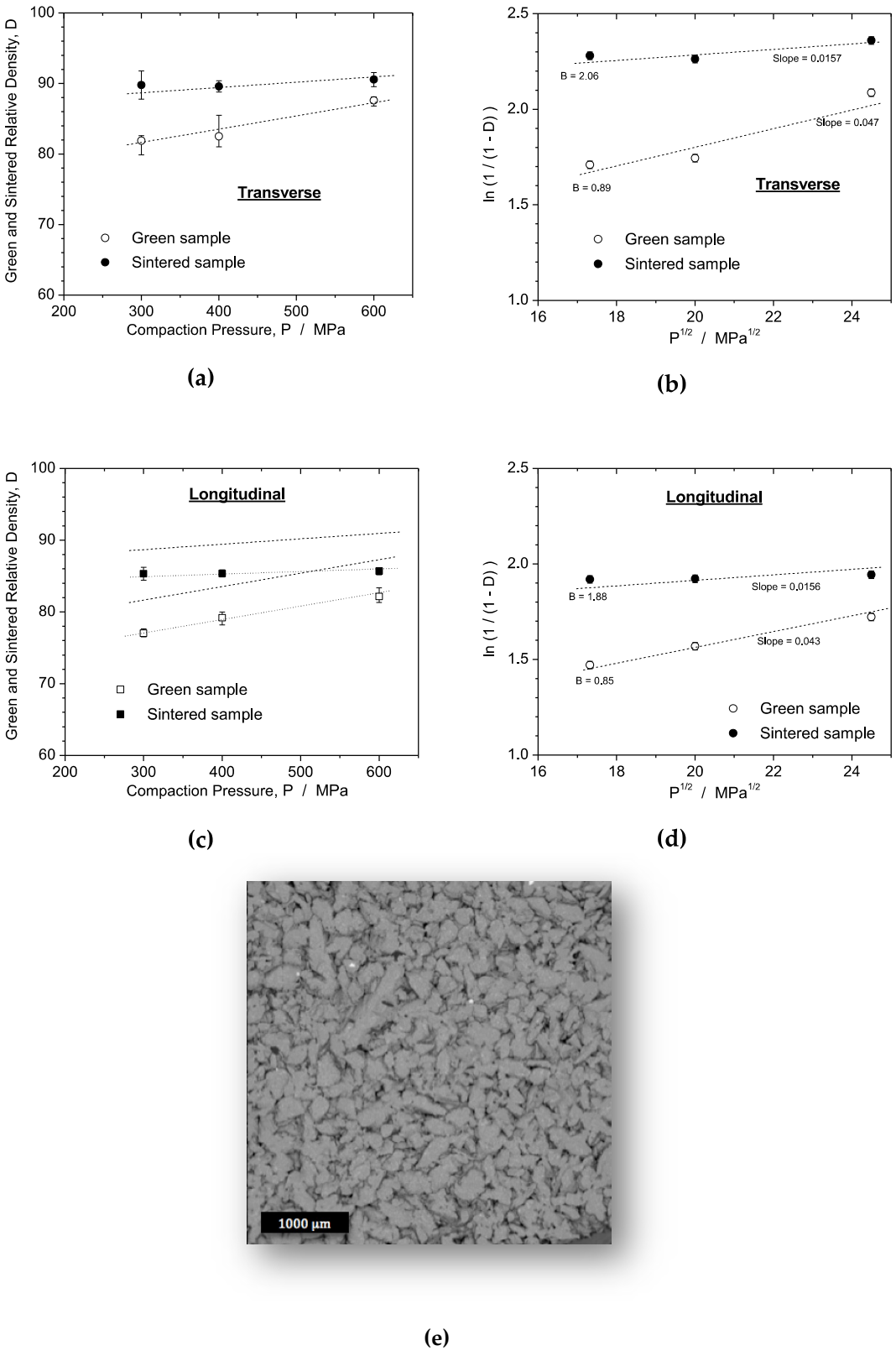

Figure 4. The experimental results of compressibility of the green and sintered Al–4Cu alloy depicting the relative densities with compaction pressures and the same data fitted by Equation #1 considering: **(a,b)** The transverse and **(c,d)** longitudinal samples. Typical micrograph depicting the porosity level of a transversal sample compacted at 600 MPa and sintered.

 doi:10.20944/preprints202309.0202.v1

Although other equations, such as the Heckel equation [20, 27-28] and double logarithmic equations [28], have been proposed to describe densification with compaction load or pressure, as described by Equation #3 [20]:

$$\ln (1/(1-D) = AP^{½} + B \quad (3)$$

where D is the density of sample and P is the used pressure, and A and B are constants corresponding to the densification coefficient related to the plastic deformation of particles and the proportionality constant, respectively [20; 27-28].

Figure 4(c) and 4(d) present similar data to Figure 4(a) and 4(b), representing the compressibility curves fitted using Equation #3 for the longitudinal samples. All straight lines show a good linear correlation coefficient when comparing the experimental data, with coefficients higher than 0.94.

Using Equation #3, it has been reported [20; 28] that parameters A (slope of the line) and B (intercept of the curve at zero pressure) represent powder plastic deformation and density without pressure (apparent density), respectively. Comparing both the transverse and longitudinal samples, the green samples have higher slopes, namely 0.047 and 0.043, compared to the sintered samples, which have slopes of 0.0157 and 0.0156, respectively, as shown in Figure 4(b) and 4(d). This suggests the distinct deformation capacities, favoring the green samples as expected. Additionally, it is observed that the densities increase and the slopes of the curves decrease with the increase of the compaction pressure, as previously reported [17-18; 20; 28].

When comparing sintered transverse and longitudinal samples, very similar slopes (parameter A) are obtained, namely 0.0157 and 0.0156, respectively. This indicates similar deformation capacity behavior in these examined samples. This similarity can be attributed to the comparable particle sizes, chemical composition, morphology, and the application of equal compaction pressures. The only difference between the examined samples is the compaction volume, with longitudinal samples compacted using a higher volume (3g compared to 1g). This seems to have a greater effect on parameter B (apparent density at zero pressure), which is slightly higher for the transverse samples (~2.06) compared to the longitudinal samples (~1.86) [20; 28]. This represents a difference of about 10%, which can be interpreted as a technical tie considering the error ranges of the experimental values.

Figure 4(e) depicts a typical SEM micrograph evidencing the porosity level attained when a transversal sample compacted at 600 MPa and sintered is characterized. Although is not commonly used a micrograph to determine the densification level, it can clearly be understood the relation between mechanical behavior and densification, as will forwardly discussed. In a previous investigation [29], by using SEM images associated with threshold images technique (ImageJ® software), the porosity level was determined. Te results shown a good similarity with those densification levels determined by using Archimedes' method.

Considering the densification levels, the highest average relative densities are observed in the sintered samples, approximately 90% compared to around 87% for the longitudinal compacted samples. This suggests that the compaction direction plays an important role in the resulting densification and mechanical behavior.

Fogagnolo et al [20] have reported distinct sliding and cold-welding behavior during the compaction of spheroidal and flattened particles. When an asymmetrical-opposed force is applied, mainly involving flattened particles, sliding and cold-welding occur at the contact points between the particles. On the other hand, when more spheroidal particles are compacted, mainly symmetrically opposed forces prevail, and no sliding and cold-welding occur. Fogagnolo et al [20] have also demonstrated that spheroidal particles have a lower parameter A (slope of the line), indicating lower deformation capacity compared to flattened particles.

It has been previously reported that spheroidal particles exhibit greater variation in accumulated energy compared to flattened particles, as compaction leads to a decrease in volume energy and an increase in surface energy [7; 18-19]. Therefore, flattened particles have a lower energy recovery since the initial energy accumulation during compaction is lower [17-19]. As a result, better energy dissipation occurs due to the randomness in filling the matrix. Consequently, the surface areas of

 doi:10.20944/preprints202309.0202.v1

interaction between particles affect energy recovery. Spheroidal particles mainly interact at the tangent point, while flattened particles interact with a larger contact area, leading to higher densification [6-7]. It was reported [17] that the compaction of fine particles in aciculate or needles-shape powders, provides better compaction than spheroidal particles. The compaction of fine particles in acicular or needle-shaped powders has been reported to provide better compaction than spheroidal particles [16; 28-31]. In this present investigation, a similar (with length of about 290 μm and width ~160 μm, as forwardly detailed) of morphology and particle size distribution is adopted, as demonstrated in Figure 3. It is important to note that the main objective is to use two distinct die compactions with equal levels of compaction pressures, while differentiating only the compaction directions. In the next section, the anisotropic effects on the resulting tensile and compressive strengths will be evaluated.

3.2. Anisotropic Effect on Morphology of Compacted Particles

It is important to note that the images shown in Figures 5 and 6 correspond to the morphologies of the compacted and sintered samples. The sintering process involves solution treating, water quenching, and natural aging (T4), as described in the experimental section. The observed surface fractures are preserved after the tensile testing measurements. It is also worth mentioning that no substantial modifications in morphologies and powder size distributions are observed when analyzing groups, I and II.

Figure 5(a) shows a typical image (SEM using backscattered electrons, BSE) of a surface fracture of the Al–4Cu alloy compacted and sintered perpendicularly to section AA. The compacted particles in this section appear relatively more spheroidal compared to section BB (Figure 6). These samples are designated as the "LONGITUDINAL" due to the applied compaction direction being perpendicular to section AA. The ghost lines indicate the trend towards a spheroidal-like morphology of these resulting particles. Figure 5(b) shows a typical observation at section BB (also using BSE technique). It shows a resulting morphology of the compacted samples that is more flattened or elongated compared to section AA.

Figure 6(a) and (b) depict the resulting morphologies of the Al–4Cu alloy composites. These SEM images (BSE) show two distinct sections, CC and DD. These samples are designated as "TRANSVERSE" as the applied tensile testing load is perpendicular (transversal) to the compaction loads, as shown in Figure 1(b). Unlike the longitudinal samples, the transverse samples exhibit a predominance of more elongated or flattened powder particles.

When correlating the resulting morphologies shown in Figures 5 and 6 with the compressibility results of the Al–4Cu samples (Figure 4), it is observed that the different compaction directions lead to different resulting morphologies. Although both longitudinal and transverse samples show very similar plastic deformation capacities represented by the slope shown in Figure 4, it is suggested that the more flattened morphology observed in the transverse samples implies an anisotropic effect on the examined compacted samples. These observations are consistent with the statements provided by Fogagnolo et al [20] in their investigation of Al powder alloys.

It is worth noting that Galen and Zavaliangos [7] have also investigated both the ductile and brittle powders. They have found distinctive anisotropic strengths. They concluded that for ductile powders, higher strength results are observed in the transverse direction due to increased crack deflection resulting from higher particle overlap compared to the longitudinal direction. On the other hand, for brittle powders, the particle fragmentation occurring along the compaction direction weakens the strength in the transverse direction. In both cases, the strength anisotropy is a function of the density, although the trends are opposite, with the ductile materials becoming anisotropic and the brittle materials becoming isotropic as the density is increased. Based on these findings, the subsequent sections will examine the resulting mechanical strengths in relation to morphology, compaction directions, and the distinct heat treatments applied.

Preprints (www.preprints.org) | NOT PEER-REVIEWED | Posted: 5 September 2023 doi:10.20944/preprints202309.0202.v1

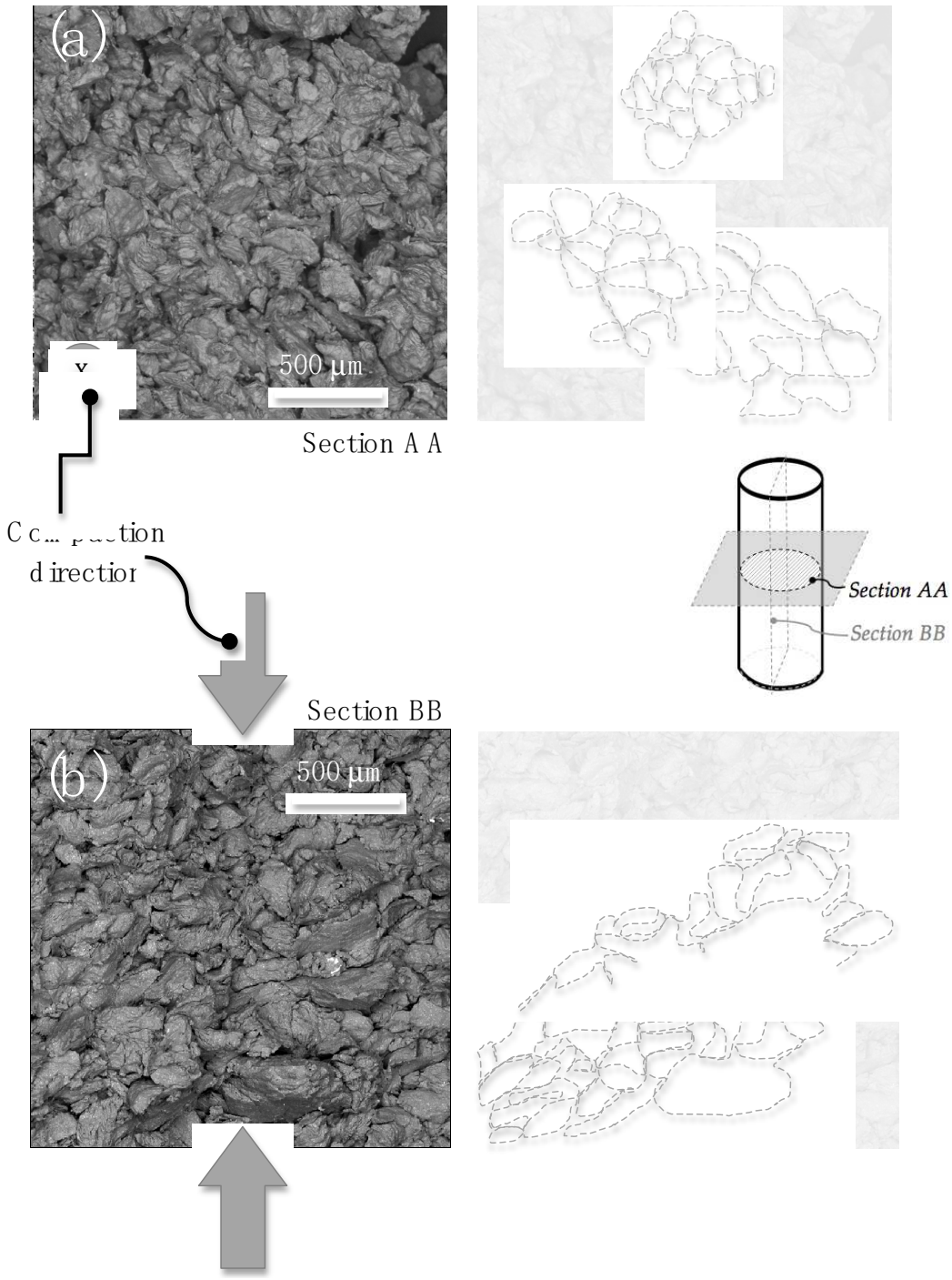

Figure 5. (a) Typical surface fracture (SEM using backscattered electrons) of the Al–4Cu composite alloy compacted perpendicularly to section AA. Typical image of the resulting flattened particles obtained in section BB, i.e. longitudinal to axis of the sample and compaction direction. These samples are designated as the LONGITUNAL samples. Arrows indicate the direction of the compaction applied. The ghost lines show the trend to morphology of the resulting particles.

Preprints (www.preprints.org) | NOT PEER-REVIEWED | Posted: 5 September 2023 doi:10.20944/preprints202309.0202.v1

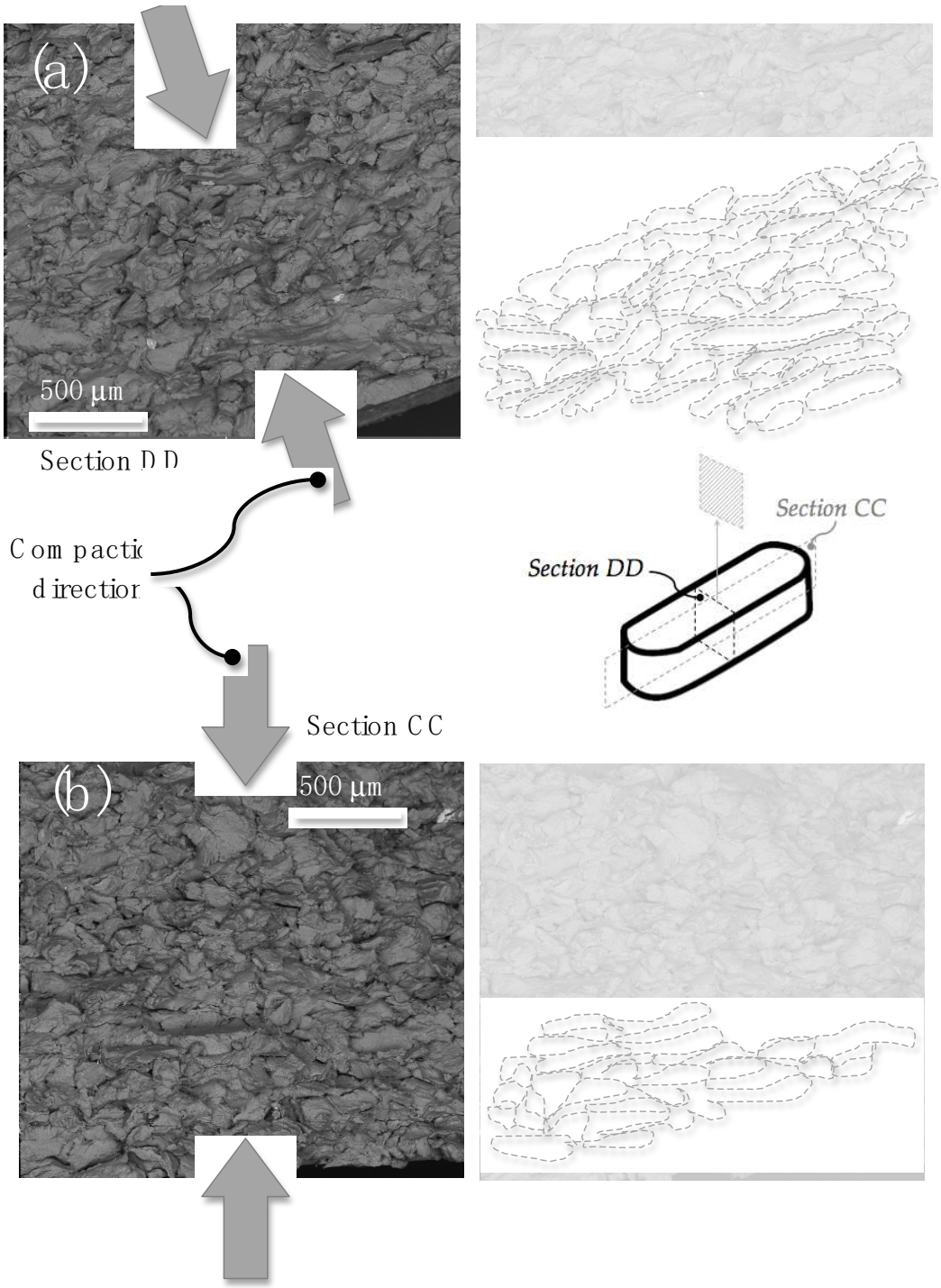

Figure 6. (a) Typical surface fracture of the Al–4Cu composite alloy compacted parallel to section DD (SEM images by using backscattered electrons). Both sections CC and DD evidence typical images of the flattened particles of the samples designated as the TRANSVERSAL samples. Arrows indicate the direction of the compaction applied. The ghost lines show the trend to morphology of the resulting particles.

3.3. Anisotropic and Mechanical Properties

3.3.1. Tensile Strengths and Heat Treatments

Figure 7 shows the experimental results of the tensile strength obtained from examining both transverse and longitudinal samples. Figure 7(a), (b), and (c) demonstrate the tensile strength results of the transverse samples as a function of the three different compaction pressures. Initially, five

Preprints (www.preprints.org) | NOT PEER-REVIEWED | Posted: 5 September 2023 doi:10.20944/preprints202309.0202.v1

experiments were conducted to ensure reproducibility. In Figure 7(c), quadruplicate results are shown due to one result being missed. Since reproducibility was observed, only duplicate results for the longitudinal samples were considered. It is important to note that no statistical treatments are commonly used, and at least duplicate results are sufficient to guarantee reproducibility. Figure 7(d), 7(e), and 7(f) display the tensile strength results for the longitudinal samples at compaction pressures of 300, 400, and 600 MPa. All the results in Figure 7 consider that the samples were only sintered at 540°C for 1 hour and subsequently air-cooled (~27°C). Therefore, the tensile strengths considering compaction pressure, direction, and sintering at 540°C can be analyzed.

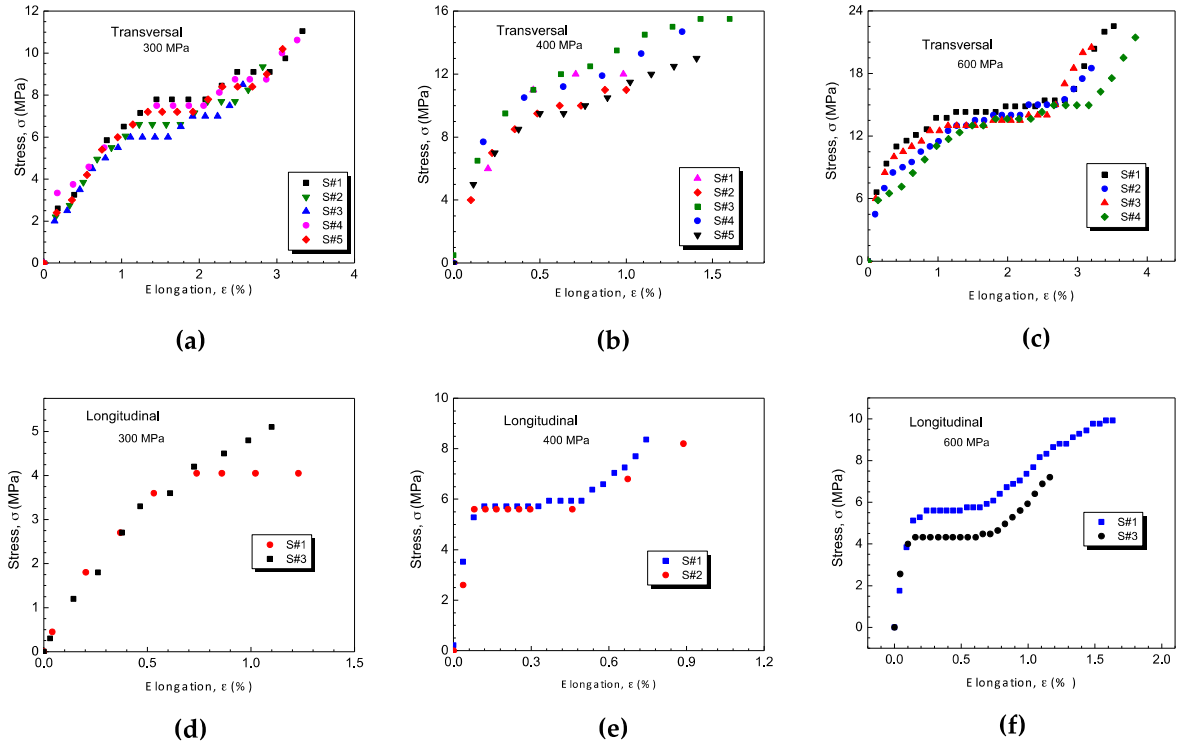

Figure 7. The experimental results of tensile strengths (stress vs. strain) of the sintered the Al–4Cu composite samples which were compacted at transverse direction using: (a) 300 MPa, (b) 400 MPa and (c) 600 MPa and all sintered at 540 °C for 1h. The stress vs. strain curves of the Al–4Cu composite samples compacted at longitudinal direction using: (d) 300 MPa, (e) 400 MPa and (f) 600 MPa and also all sintered at 540 °C for 1h.

Figure 8 summarizes the obtained results from examining both transverse and longitudinal samples, corresponding to the tensile strengths of the Al–4Cu samples after sintering followed by water quenching and subsequent natural aging (T4) for approximately 30 days. Figure 8(a), (b), and (c) show the triplicate results of the transverse Al–4Cu samples for compaction pressures of 300, 400, and 600 MPa, respectively. Figure 8(b) represents the concatenated results of the longitudinal samples, which are representative of the triplicate/duplicate results.

Table 1 provides a comparison and discussion of the tensile strengths of both the transverse and longitudinal samples of the Al–4Cu composites. For the sintered samples, an increase of approximately 30% in compaction pressure (from 300 to 400 MPa) leads to a quasi-linear increase in ultimate tensile strength (UTS) from 11 to 15 MPa. Similarly, when the compaction pressure is increased from 400 to 600 MPa (1.5x), the same linear trend is observed. This indicates that doubling the compaction pressure results in an approximately 2x increase in UTS. However, there are limitations to consider, such as the dimensions of the components and dies inside the press, as well as the feasibility of acquiring a press with high pressing capacity. It is worth noting that the compaction pressures ranging between 100 and 600 MPa are commonly practiced in industrial applications.

Preprints (www.preprints.org) | NOT PEER-REVIEWED | Posted: 5 September 2023 doi:10.20944/preprints202309.0202.v1

Table 1. Summarized values of YS (yield strength), UTS (ultimate tensile strength) and elongation (ε) obtained from the stress vs. strain curves of the sintered (at 540 °C for 1h) and sintered and T4 heat-treated samples in both the transverse and longitudinal compaction directions.

Samples	Sintered			Quenched + T4		
Transversal	**YS, MPa**	**UTS, MPa**	**ε, %**	**YS, MPa**	**UTS, MPa**	**ε, %**
300 MPa	7 (± 1)	11 (± 1)	3.5 (± 0.2)	4 (± 0.5)	14 (± 1)	18 (± 0.2)
400 MPa	10 (± 0.5)	15 (± 1)	1.5 (± 0.2)	3.5 (± 0.5)	18 (± 1)	19 (± 0.2)
600 MPa	14 (± 0.5)	23 (± 1)	3.6 (± 0.2)	3.0 (± 0.5)	34 (± 2)	23 (± 0.2)
Longitudinal	**YS, MPa**	**UTS, MPa**	**ε, %**	**YS, MPa**	**UTS, MPa**	**ε, %**
300 MPa	4.0 (± 0.5)	6 (± 1.0)	0.9 (± 0.2)	4.5 (± 0.5)	6.5 (± 0.5)	0.8 (± 0.1)
400 MPa	4.5 (± 0.5)	8 (± 0.5)	0.8 (± 0.2)	3.5 (± 0.5)	7.5 (± 0.5)	1.2 (± 0.1)
600 MPa	4.5 (± 0.5)	10 (± 0.5)	1.3 (± 0.3)	4.5 (± 0.5)	10 (± 0.5)	1.5 (± 0.2)

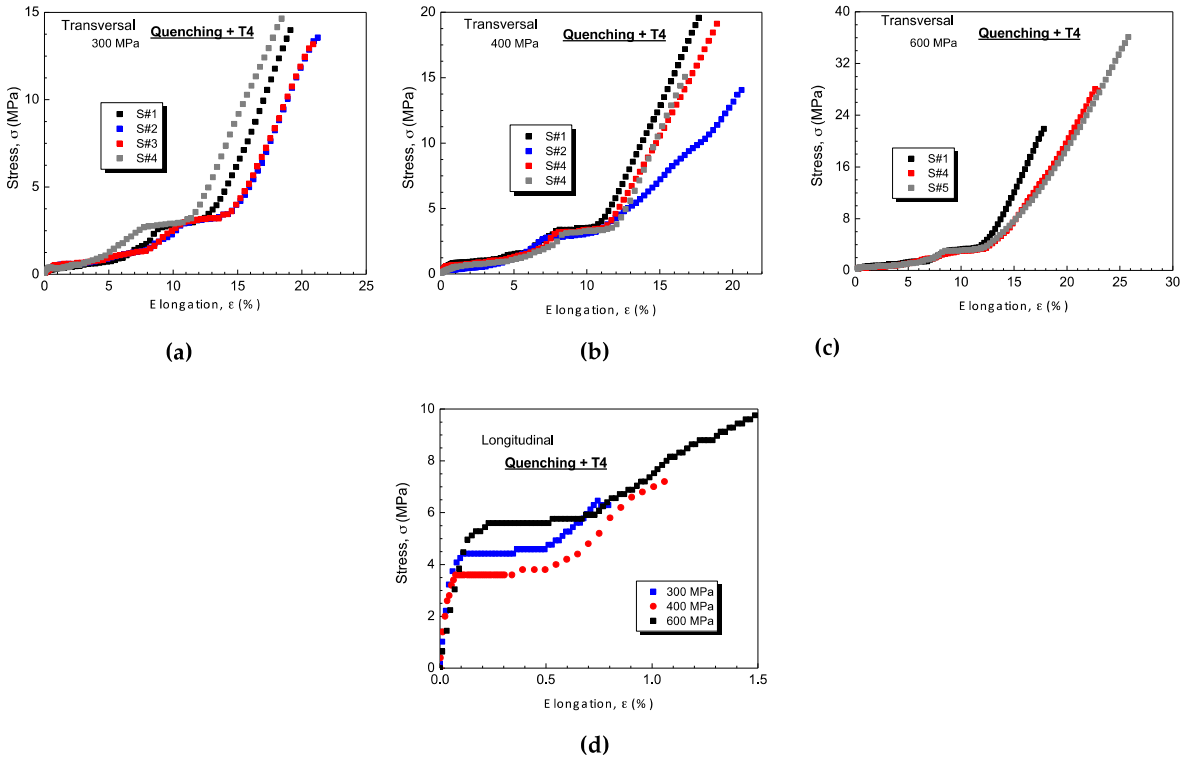

Figure 8. The experimental results of tensile strengths (stress vs. strain) of the sintered (at 540 °C for 1h) and T4 heat-treated Al–4Cu composite samples using 300 MPa, 400 MPa and 600 MPa: (a), (b) and (c) corresponding with transverse samples and (d) concatenate the three distinct compaction pressures.

The UTS values of the longitudinal samples also increase by approximately 1.5x with an increase in compaction pressure. However, the UTS and elongation (e) values of the transverse samples are approximately 2x higher than those of the longitudinal samples. The yield strength (YS) results of the longitudinal samples are not affected by the compaction pressure, which seems to be associated with the compaction direction and the resulting anisotropy.

Previous studies [7; 18-19] have reported that during tension in the transverse direction, a bridging effect is prevalent. This effect causes cracks to not only change their direction (deflection) but also strive to propagate through the elongated particles in the transverse direction. A frictional resistance is induced, and the contacts perpendicular to the direction of compaction become larger compared to those along other directions [7].

 doi:10.20944/preprints202309.0202.v1

It should be noted that the obtained UTS values are relatively lower compared to those commonly achieved in as-cast alloys. Gokçe and Findik [32] have also obtained similar UTS values when investigating Al powder composites. In this mentioned study, when compaction pressure of 490 MPa and sintering for 2 h are applied, a densification of about ~91% is attained. It is also remarked that when a sintering during 6 h is carried out, in this mentioned study developed by Gokçe and Findik [32], the tensile strengths have attained of about 240 MPa. Low UTS (~15 MPa) are also attained for atomized Al powders, when a conventional powder metallurgy route is adopted [33].

In this study, the focus is on the effect of anisotropy, considering the effects of distinct compaction directions on the mechanical responses. It is important to mention that Galen and Zavaliangos [7] have also examined the degree of anisotropy in low alloy steel powder and obtained lower tensile strengths compared to those commonly achieved in as-cast low alloy steel. From this perspective, no novelty is provided. However, when the heat treatment is associated with the possibility of using powder particles from recycling processes, an environmentally-friendly aspect can be considered. It is also important to emphasize the need for systematic planning of the mechanical forces (compressive or tensile, or combined) in the final application.

When examining the experimental results of the transverse and T4-treated samples, it appears that UTS and elongation are improved. However, this improvement is more pronounced when a compaction pressure of 600 MPa is applied. This is due to the UTS results being technically similar at compaction pressures of 300 and 400 MPa. On the other hand, an increase of approximately 25-30% and 6x is observed in UTS and elongation, respectively, when a compaction pressure of 600 MPa is applied.

Although it is widely recognized that a naturally aged sample increases substantially the mechanical behavior, when using powder particles compacted, sintered and heat treated (T4), the applied compaction pressure has also an important hole on the final properties. This seems to be associated with the elongated particles generating the "bridging effects" affecting mainly the resulting elongation. However, it is remarked that other microstructural parameters synergistically contribute to improve the mechanical response, as occurs commonly in an as-cast material (e.g. solute content, dendritic spacings, second phase, etc.). The same mechanism helps to understand the substantial increasing into the elongation. Galen and Zavaliangos [7] have also observed that at transversal direction, the bridging effect is amplified. This offers a higher frictional resistance of the sides of the elongated particles than the longitudinal samples.

When the longitudinal samples are evaluated, the T4 heat-treating has no provided any beneficial effect on the resulting properties. This seems also to be associated with the morphology of the compacted particle. Comparing the resulting morphologies depicted in Figures 5 and 6, it is slightly observed that the longitudinal samples tend to more spheroidal than those transverse samples. This corroborates with the understanding of the bridging effect previously mentioned.

It is worth noting that the effect of the heat-treatment improving the mechanical behavior depends on the compaction direction, and the anisotropic strength is evidenced. However, two points should be elucidated. A first concerns to verify the anisotropic in the compressive behavior and another is to confirm the constituted phases when T4 treatment is carried out. This due to a resulting microstructural array commonly contains different phases of the Al_2Cu phases (e.g. θ, θ , θ''). These are related to coherent, semi coherent and incoherent with respect to Al–rich matrix. These substantially affect the final properties. In the next section the anisotropic compressive strengths associated with the heat treatments are evaluated and discussed.

Although it is widely recognized that natural aging leads to substantial improvements in mechanical behavior, when using the compacted, sintered, and T4-treated powder particles, the applied compaction pressure also plays an important role in the final properties. This can be attributed to the bridging effects generated by the elongated particles. The same mechanism helps to explain the significant increase in elongation. Galen and Zavaliangos [7] have also observed that in the transverse direction, the bridging effect is amplified, resulting in higher frictional resistance along the sides of the elongated particles compared to the longitudinal samples.

Preprints (www.preprints.org) | NOT PEER-REVIEWED | Posted: 5 September 2023 doi:10.20944/preprints202309.0202.v1

When evaluating the longitudinal samples, it is observed that the T4 heat treatment does not provide any beneficial effect on the resulting properties. This can also be associated with the morphology of the compacted particles. Comparing the resulting morphologies depicted in Figures 5 and 6, it is slightly observed that the longitudinal samples tend to be more spheroidal compared to the transverse samples. This supports the understanding of the bridging effect mentioned earlier.

It is important to note that the effect of heat treatment in improving mechanical behavior depends on the compaction direction, and the anisotropic strength is evident. However, there are two remaining points to elucidate. Firstly, it is necessary to verify the anisotropy in compressive behavior. Secondly, the constituted phases during T4 treatment need to be confirmed and compared with samples that were only sintered. This is because the resulting microstructural array commonly contains different phases of Al_2Cu, which can be coherent, semi-coherent, and incoherent with respect to the Al-rich matrix. These phases can substantially affect the final properties. The next section will evaluate and discuss the anisotropic compressive strengths associated with heat treatments.

3.3.2. Compressive Strengths and Heat Treatments

Figures 9(a) and 9(b) display the typical results of the compressive tests on transverse samples that were sintered and T4 treated. Two different positions (P1 and P2) are shown in Figure 1(e) when considering the transverse position with respect to the compaction direction. These P1 and P2 samples demonstrate very similar reproducibility.

Figures 9(c) and (d) illustrate the compressive strengths of both transverse and longitudinal samples after T4 treatment, considering three distinct compaction pressures. Table 2 provides a comparison of the resulting ultimate compressive strength (UCS) values between sintered and T4 treated samples.

Table 2. The average values of UCS (ultimate compressive strength), YS (yield strength) and load applied in diametrical compression (DC) inducing to indirect tensile strength for the sintered and T4 heat-treated samples in transverse and longitudinal directions. All samples are sintered at 540 °C and water quenched followed by a T4 treatment.

Samples	Sintered		Quenched + T4			
TRANSVERSAL	**YS, MPa**	**UCS, MPa**	**YS, MPa**	**UCS, MPa**	**F, N**	**DC***
300 MPa	65 (± 5)	118 (± 6)	92 (± 5)	165(± 10)	---	---
400 MPa	80 (± 10)	135 (± 10)	118 (± 5)	195 (± 10)	---	---
600 MPa	105 (± 8)	175 (± 8)	150(± 10)	270 (± 10)	---	---
LONGITUDINAL	**YS, MPa**	**UCS, MPa**	**YS, MPa**	**UCS, MPa**	**F, N**	**DC***
300 MPa	15 (± 2)	28 (± 5)	63 (± 5)	75 (± 6)	0.9 (± 0.2)	8.6 (± 3)
400 MPa	35 (± 2)	55 (± 5)	85 (± 5)	110 (± 8)	1.2 (± 0.2)	11.6 (± 3)
600 MPa	48 (± 4)	80 (± 8)	95 (± 10)	145 (± 10)	2.3 (± 0.1)	23.2 (± 0.8)

As expected, similar to the tensile strengths, increasing the compaction pressure by approximately 1.5 times also increases the compressive response by approximately 1.5 times. The transverse samples exhibit UCS values that are higher, at least 2 times, compared to the longitudinal samples, as shown in Table 2. Additionally, the UCS values are at least 1.2 times higher than the yield strength (YS). It is worth noting that the YS values are obtained when the region called the "quasi-linear elastic" domain is initiated. Similar UCS values were also observed for an Al-5 wt.% Cu composite using 430 MPa [17; 19].

Preprints (www.preprints.org) | NOT PEER-REVIEWED | Posted: 5 September 2023 doi:10.20944/preprints202309.0202.v1

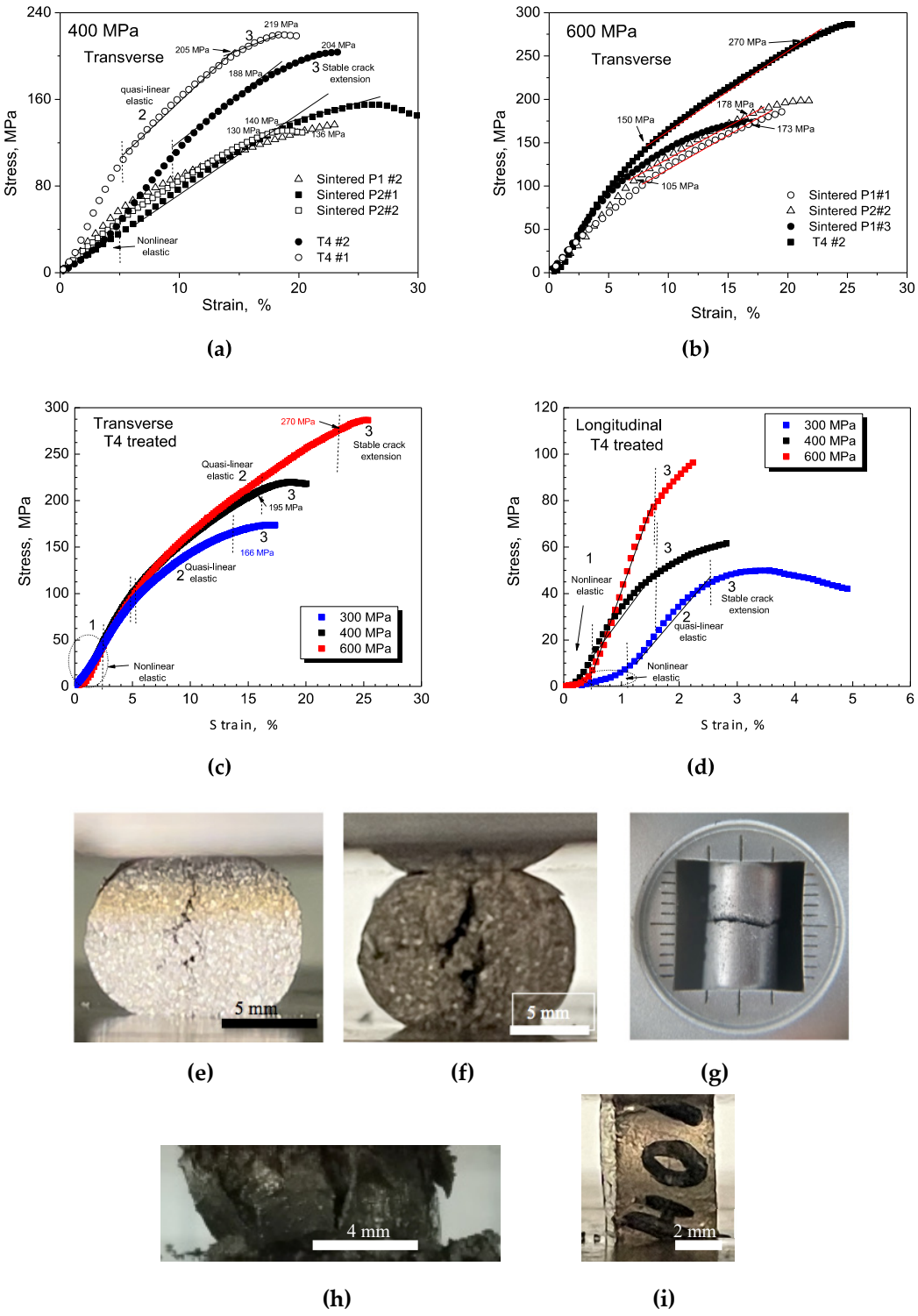

Figure 9. The experimental results of compressive strengths (stress vs. strain) of the sintered (at 540 °C for 1h) and T4 heat-treated corresponding with: **(a)** transverse at 400 MPa, **(b)** 600 MPa, and after T4 treatment for the transverse **(c)** and longitudinal samples **(d)**. Typical pictures showing cracks initiating **(e)** at vertical position, which is collinear with compaction load direction, end of test **(f)**, and a typical example of a cylindrical specimen (longitudinal samples) after the tensile testing **(g)** and after compressive testing **(h)**, and after "barriling" in compressive test of the transverse sample.

It is important to note that diametrical compression was carried out on the longitudinal samples based on the Hertz equation, as previously reported [7; 32-33]. Table 2 indicates that $DC = 2 \cdot F / \pi \cdot L \cdot D$, which corresponds to diametrical compression, where F, L, and D are the load at failure, initial length, and diameter of the sample [7].

 doi:10.20944/preprints202309.0202.v1

According to Galen and Zavaliangos [7], the Hertz equation is valid for isotropic elastic materials that undergo brittle failure. The proposed composite, consisting of compacted and sintered particles, exhibits this mechanical behavior. This is evident when comparing the calculated results of DC (Table 2) with the tensile strength results obtained from transverse samples. Therefore, even though the longitudinal samples are compacted in the longitudinal direction, the indirect tensile strength (DC) yields similar values to the transverse samples tested under perpendicular tension. This is confirmed when comparing the error ranges and "pure" tensile strength values in Table 1 (11 ± 1, 15 ± 1, and 23 ± 1) with the DC results for compaction pressures of 300, 400, and 600 MPa, as shown in Table 2.

Figures 9(e) and 9(f) display typical images of longitudinal samples (cylindrical shape) after compression. The boundaries among deformed particles are reasonably observed in Figure 9(e), and the initiated cracks in the same line or direction of the applied load are also revealed. Figure 9(g) and (h) show typical images after the tensile and compressive tests on the longitudinal samples, respectively. A typical image after a compressive test on a transverse sample is depicted in Figure 9(i). It is important to note that the compression test is stopped when a stable stress vs. strain curve is observed.

Jonsen et al [34], when investigating diametrical measurements, have demonstrated a sequence of pictures (images) related to the load curve of the material under examination. They identified the moment and position on the load curve corresponding to crack appearance. Although Jonsen et al [34] used a diagram showing force versus displacement, while in Figure 9, stress vs. strain is shown, the three distinct regions are characterized. Region 1 represents nonlinearity, followed by a quasi-linear elastic region (region 2), and finally region 3 where cracks initiate and propagate. It is noted that cracks initiate at the interface between regions 2 and 3. It is reported that the cracks grow in a stable manner through the sample, and the load reaches values corresponding to YS, while unstable crack propagation continues until a maximum value is reached. This maximum value does not represent the UCS. It is worth noting that the UCS and YS are obtained from the experimental curves by limiting regions 2 and 3 and 1 and 2, respectively. Triplicate or duplicate curves are considered, and at least three points at the interface of the mentioned regions are also considered to obtain the average value, as demonstrated in Table 2.

Both the longitudinal and transverse samples exhibit similar nonlinear regions, independent of the compaction pressure applied. This observation seems to be associated with the bridging effect mentioned earlier. Due to a high interface among elongated/deformed particles, the region corresponding to elastic (or quasi-elastic) behavior is favored in the sample with more pronounced elongated particles, as observed in Figure 9(c) and 9(d).

3.3.3. Mechanical Behavior Correlations

Figures 10(a) and 10(b) display the ultimate tensile strength (UTS) and ultimate compressive strength (UCS) as a function of the compaction pressures for both the transverse and longitudinal samples. The yield strengths in tensile and compressive tests are also shown. It is evident that the anisotropic strength is favored in the transverse samples. As expected, when comparing the UCS and UTS values, a nonlinear trend is observed, as shown in Figure 10(c). A single logarithmic equation (UCS = 64 ln(UTS) - 80) describes the trend for both longitudinal and transverse samples. This indicates that the morphology and chemical composition of the powder particles used are similar. It should be noted that an isotropic material, such as a multidirectional solidified as-cast alloy, commonly exhibits a linear equation for the UCS to UTS ratio.

The degree of anisotropy or strength anisotropy is quantified using the ratio between the maximum and minimum values of mechanical behavior, as previously reported by Galen and Zavaliangos [7; 9]. For plastically deformable materials, the anisotropy ratio is lower than 1 and decreases with increasing densification.

Figures 10(c) and 10(d) depict the strength anisotropy ratios as a function of the applied compaction pressures. The degree of anisotropy, obtained by comparing the UCS and UTS ratios between transverse and longitudinal samples, is shown. Galen and Zavaliangos [7] have also demonstrated that most materials with ductile behavior exhibit an anisotropy ratio lower than 1. The

Preprints (www.preprints.org) | NOT PEER-REVIEWED | Posted: 5 September 2023 doi:10.20944/preprints202309.0202.v1

degree of anisotropy decreases with increasing densification, i.e., increasing compaction pressure [7]. It is noteworthy that the examined samples in our study did not exhibit ratios higher than 1.

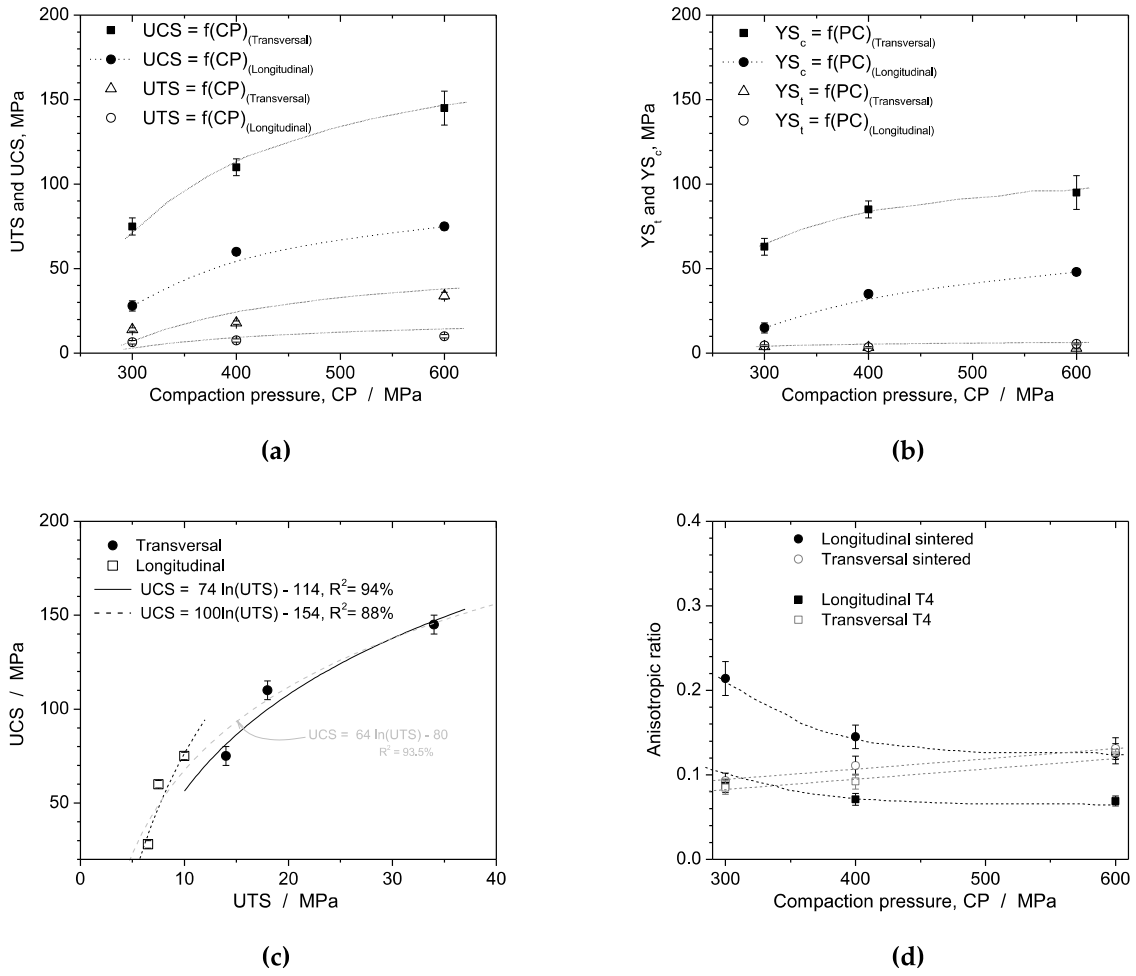

Figure 10. The experimental results of: **(a)** UTS and UCS vs. compaction pressure (CP), **(b)** yield (YSt) tensile and yield compressive (YSc) strengths vs. CP, **(c)** ratio between UCS and UTS and **(d)** the anisotropic ratio between UCS and UTS for the longitudonal and transverse samples considering both sintered and T4 treated samples.

Figure 10(d) shows the degrees of anisotropy or anisotropy ratios for both the longitudinal and transverse samples in both the sintered and quenched + T4 treated conditions. Table 3 provides a summary of the observed tendencies. Interestingly, the longitudinal samples in sintered and T4 treated conditions exhibited decreasing trends with increasing compaction pressures. Conversely, the transverse samples in sintered and T4 treated conditions showed increasing trends. Within certain limitations, it can be observed that the transverse samples become more isotropic (or less anisotropic) than the longitudinal samples. This is evident in both Table 3 and Figure 10(d). The transverse samples exhibit slightly increasing anisotropy ratios, which are very similar. In contrast, the longitudinal samples exhibit non-linear decreasing trends that are more dispersed or distant between each analyzed sample. Additionally, it can be noted that the sintered longitudinal samples are more isotropic or less anisotropic than the T4 treated longitudinal samples. Among the examined samples, the highest anisotropy ratio is observed for the T4 treated sample at 600 MPa of compaction pressure, while the other examined samples exhibit similar anisotropy ratios, which vary for other compaction pressures.

Preprints (www.preprints.org) | NOT PEER-REVIEWED | Posted: 5 September 2023 doi:10.20944/preprints202309.0202.v1

Table 3. The anisotropic ratio (AR)(*) considering both the sintered and T4 heat-treated samples with respect to longitudinal and transversal conditions versus compaction pressures.

Sintered	Longitudinal	Transversal
300 MPa	0.214	0.093
400 MPa	0.145	0.111
600 MPa	0.125	0.131
Quenched + T4	**Longitudinal**	**Transversal**
300 MPa	0.087	0.085
400 MPa	0.071	0.092
600 MPa	0.069	0.126

(*) AR = UTS/UCS considering each compaction direction, i.e. longitudinal and transversal. These values are into Tables 1 and 2.

Galen and Zavaliangos [7] observed that strength anisotropy becomes more pronounced with increasing density, which is achieved through increasing compaction. In our investigation, this is only observed for the longitudinal samples. Galen and Zavaliangos [7] also noted that the same material with a non-equiaxed (acicular) morphology exhibits higher anisotropy than the same material with equiaxed morphology.

In our study, the resulting morphology of the compacted powders in the longitudinal samples is more spheroidal than in the transverse samples. This observation is consistent with the findings of Galen and Zavaliangos. Xu et al [9] determined the degree of anisotropy using the Young's modulus and compressive strength and found that the degree of anisotropy decreases with increasing compaction pressure. In our experiment, this trend is only observed in the longitudinal samples. Based on these observations, it can be concluded that the morphology, compaction pressure, and heat treatment affect the strength anisotropy.

When comparing the X-ray diffraction (XRD) patterns, the green, sintered, and T4 treated samples exhibit very similar phases. Figure 11(a) shows the XRD analysis of the green powder samples, sintered powders, and T4 treated powders, which were obtained from drilled compacted and treated specimens. The diffraction intensity reveals that the peaks corresponding to Al crystallographic planes (111), (200), (220), (311), and (222) (JCPDS # 01-1180) are present. Figure 11(b) shows that between angles 15º and 50º, the Bragg's planes (110), (200), (210), (211), (403), (220), (112), (310), and (202) (JCPDS # 01-1180), which correspond to Al_2Cu intermetallic crystallographic planes, are present, as previously reported [17; 19, 35-38]. It is also observed that the coherent Al2Cu phases designated as θ' and θ'' are not substantially identified at angles ~23º and ~31º [17; 38].

The XRD pattern of the T4 treated sample differs mainly in the presence of the main θ Al_2Cu phases, specifically at (111), (220), (112), (310), and (202). These phases are clearly observed in both the sintered and as-green samples, but not substantially in the T4 treated sample. Figure 11(c) presents the XRD patterns of the green sample in both powder and consolidated conditions (samples #1 and #2). It is important to note that the powder sample is obtained from the as-cast alloy after drilling. The consolidated samples are obtained after compaction (e.g., using 600 MPa), and samples #1 and #2 represent the top and bottom analysis of the same sample, respectively.

These comparisons aim to clarify that no substantial differences are observed when comparing samples in powder and consolidated (or compacted) conditions. The compacted samples exhibit more pronounced peaks corresponding to the θ' and θ'' phases, as well as other phases at angles higher than 50 º, as shown in Figure 11(c). Additionally, Figure 11(d) confirms that the XRD patterns remain unchanged after heat treatment and testing under compressive loading.

The most significant modifications are observed in the intensity decrease of peaks related to the incoherent Al_2Cu in the planes (110) and (200) at ~21 ° and ~29 °, as depicted in Figure 11. This can be attributed to the fact that during the solution treatment, a homogeneous solid solution (α-Al phase) with Cu dissolved in the Al matrix is formed. Subsequently, the quenching leads to the formation of

Preprints (www.preprints.org) | NOT PEER-REVIEWED | Posted: 5 September 2023 doi:10.20944/preprints202309.0202.v1

a supersaturated solid solution of the θ phase. This mechanism is commonly described in the literature [35-38]. It is reported that a typical transition in Al–Cu alloys is from a supersaturated solution to coherent GP (Guinier Preston) zones, followed by intermediate coherent (θ'') and semi-coherent (θ') phases, and finally to a more stable (θ) phase [36; 38]. Based on these observations and the analysis of the XRD patterns, it can be inferred that the T4 treated samples have a partial dissolution of their Al_2Cu phases, mainly those corresponding to the planes (110) and (200) at ~21 ° and ~29 °. Additionally, the intensity peaks of Al (e.g., at planes (111), (200), and (220)) have proportionally and comparatively increased, suggesting the dissolution of Cu and the formation of a supersaturated solution along with some remaining Al_2Cu phases. It is worth noting that the complete dissolution or subsequent precipitation did not occur after a water quenching or a natural aging. These findings help to explain the improved mechanical behavior.

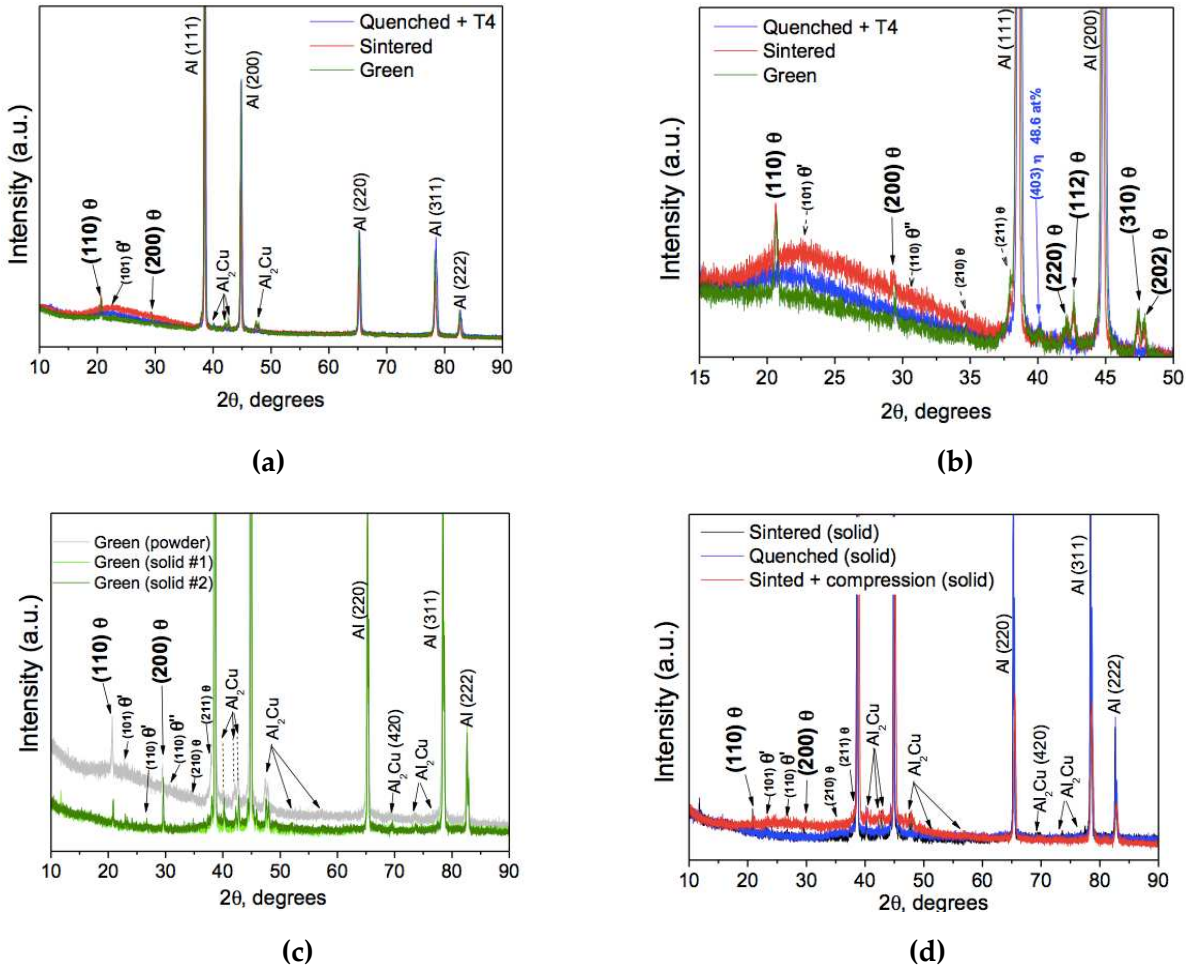

Figure 11. Typical XRD patterns of: (**a**) the green, sintered and T4 treated sample, **(b)** evidencing phases between 15 and 50 °, **(c)** the green samples after compaction stage characterizing top and bottom surfaces (samples# 1 and #2), and (**d**) showing that no substantial differences in constituted phases are attained after sintering, T4 treatment and after sintering followed by compressive test under 600 MPa.

Zhang et al [38] recently demonstrated the presence of the three distinct Al_2Cu phases, i.e., θ' and θ'', in as-cast 2219 Al–Cu alloys. The TEM images revealed that the θ phase has a more spheroidal shape (5 to 10 μm) compared to the θ' and θ'' phases, which exhibit a needle-like morphology and are finer than the θ phase. Zhang et al [38] also found that after a solution treatment at 538 °C for 2 hours, which is similar to the treatment applied in this study (540 °C for 1 hour), both the θ' and θ'' Al_2Cu intermetallics are completely dissolved into the Al matrix. The UTS results obtained by Zhang et al [34] are similar to those obtained in this study. It is important to note that the 2219 Al–Cu alloy

 doi:10.20944/preprints202309.0202.v1

used by Zhang et al [38] has a higher Cu content, which can contribute to the enhanced mechanical behavior. Additionally, the alloy samples were cast using ultrasonic casting [38], resulting in a finer microstructural arrangement and, consequently, improved mechanical behavior. This comparison is made only to demonstrate the presence of θ' and θ'' Al_2Cu phases and their dissolution during the solution and heat treatments.

4. Conclusions

The experimental results obtained from compacted and treated Al–Cu alloy powders lead to the following conclusions:

- Different compaction directions (longitudinal and transverse) result in distinctive morphologies of the compacted powders, with spheroidal-like and elongated-like shapes. These morphological differences contribute to a "bridging effect" among the powder particles, leading to different mechanical behaviors. The sintered transverse and longitudinal samples exhibit similar deformation capacity behavior based on Heckel's equation, but the sintered samples achieve higher densification (~90% compared to ~87% for longitudinal samples). Thus, compaction direction plays a significant role in densification and resulting mechanical behavior.
- T4 treated samples consistently exhibit the highest values of ultimate tensile strength (UTS) and ultimate compressive strength (UCS) compared to other experimental conditions. The UCS values are higher than the UTS values, as expected. Transverse samples generally demonstrate better mechanical performance than longitudinally compacted samples.
- Anisotropic ratios, which represent the degree of anisotropy, are determined by comparing the maximum values of UCS and UTS for each compaction direction and heat treatment condition. Transverse samples show similar anisotropic ratios with a slight increasing trend as the compaction pressure increases. In contrast, longitudinal samples exhibit non-linear decreasing trends in anisotropic ratios with increasing compaction pressure. The ratios for longitudinal samples are more dispersed compared to transverse samples. Therefore, sintered longitudinal samples are more isotropic or less anisotropic than T4 treated longitudinal samples.
- The resulting morphology of the longitudinal samples, which is more spheroidal compared to transverse samples, is associated with the compaction direction. This finding indicates that the initial morphology, compaction load, and heat treatment affect the strength anisotropy. Recycled powder particles from conventional machining processes can potentially be used, allowing for the production of components with specific mechanical requirements through careful compaction planning and treatments. These approaches offer environmental benefits by eliminating metallic fumes and reducing electrical energy consumption associated with melting processes.

Overall, the study demonstrates the influence of compaction direction and heat treatment on the mechanical behavior and anisotropy of Al–Cu alloy powders. It highlights the potential for using recycled powder particles and environmentally friendly production methods in the manufacturing of components with desired mechanical properties.

Author Contributions: R.S.B. has prepared and treated all samples. R.S.B., R.F.G.B. and E.P have carried out the mechanical characterization, organized the data and correlated with attained results of all examined specimens. A.D.B. and E.P. have carried out the XRD measures and organized and treated the data attained. He has also helped with the general organization and with the English written manuscript. W.R.O., R.S.B, A.D.B and E.P. have contributed with the general organization of the experimentations and analyses and correlations. W.R.O. and A.D.B have also written and organized the proposed manuscript. All authors have read and agreed to the published version of the manuscript.

Funding: The financial support provided by FAEPEX-UNICAMP (#2252/23), CAPES (Coordination for the Improvement of Higher Education Personnel), Ministry of Education, Brazil, Grant #1) and CNPq (The Brazilian Research Council) Grants, #407595/2022-8; #313272/2021-2 and 310010/2020-9.

Institutional Review Board Statement: Not applicable

Informed Consent Statement: Not applicable

Data Availability Statement: All research data supporting this publication are directly available within this publication.

Acknowledgments: Acknowledgments are also provided to Mr. Luiz A. Garcia (technician department) whom has contributed with technical aspects and equipment organization..

Conflicts of Interest: The authors declare no conflict of interest.

References

1. Guo MX, Wang MP. Effects of particle size, volume fraction, orientation and distribution on the high temperature compression and dynamic recrystallization behaviors of particle-contaning alloys. Mat. Sci. Eng. A 546 (2012) 15-25.
2. Loidolt P, Ulz MH, Khinast J. Prediction of the anisotropic mechanical properties of compacted powders. Powder Technology 345 (2019) 589–600
3. Akisanya AR, Cocks ACF, Fleck NA. The yield behavior of metal powders. Int J Mech Sci 39 (1997) 1315-1324.
4. Vityaz PA, Sheleg VK, Kaptsevich VM, Kusin RA, Gurevich AA. Plasticity condition of anisotropic high-porosity powder materials. Poroshkovaya Metallurgiya 9 (1984) 1-5.
5. Weston JE. Origin of strength anisotropy in hot-pressed silicon nitride. J Mater Sci 15 (1980) 1568-1576.
6. Zavaliangos A, Bouvard D. Numerial simulation of anisotropy in sintering due to prior compaction. Metal Powder Rerpot 57 (2002) 39-39.
7. Galen S, Zavaliangos A. Strength anisotropy in cold compacted ductile and brittle powders. Acta Materialia 53 (2005) 4801-4815.
8. Cao L, Zeng W, Xie Y, Liang J, Zhang D. Effect of powder oxidation on the anisotropy in tensile mechanical properties of bulk Al samples fabricated by spark plasma sintering. Mater Sci Eng A 764 (2019) 138246.
9. Xu G, He C, Su A, Chen Z. Experimental investigation of the anisotropic mechanical behavior of phyllite under triaxial compression. Int. J Rock Mech and Mining Sci 104 (2018) 100-112.
10. Reis DAP, Couto AA, Domingues Jr NI, Hirschmann ACO, Zepka S, Moura Neto C. Effect of artificial aging on the mechanical properties of an aerospace aluminum alloy 2024. Defect and Diffusion Forum 326-328 (2012) 193-198.
11. Reddy TB, Karthik P, Krishna G. Mechanical behavior of Al-Cu binary alloy system/ Cu particulates reinforced metal-metal composites. Results in Eng 4 (2019) 100046.
12. Iswanto PT, Pambekti A. Heat treatment T4 and T6 effects on mechanical properties in Al-Cu alloy after remelt with different pouring temperatures. Metalurgija 59 (2020) 171-174.
13. Alexopoulos ND, Velonaki Z, Stergiou CI, Kour-koulis SK. Effect of ageing on precipitation kinetics, tensile and work hardening behavior of Al-Cu-Mg (2024) alloy. Mater Sci Eng A 700 (2017) 457–467.
14. Fernandez Gutiérrez R, Sket F, Maire E, Wilde F, Boller E, Requena G. Effect of solution heat treatment on microstructure and damage accumulation in cast Al-Cu alloys, J Alloys Compd 697 (2017) 341-352.
15. Rivera-Cerezo H, Gaona-Tiburcio C, Cabral-Miramontes J, Bautista-Margulis R, Nieves-Mendoza D, Maldonado-Bandal E, Estupiñan_lopez F, Almeraya-Calderón F. Effect of heat treatment on the electrochemical behavior of AA2055 and AA2024 alloys for aeronautical applications. Metals 13 (2023) 429. doi.org/10.3390/met13020429.
16. Satizabal LM, Caurin HFN, Meyer YA, Padilha GS, Bortolozo AD, Osório WR. Distinct heat treatments and powder size ratios affecting mechanical responses of Al/Si/Cu composites. J Comp Mater. 55 (2021) doi.org/10.1177/00219983211029.
17. Meyer YA, Bonatti RS, Costa D, Bortolozo AD, Osório WR. Compaction pressure and Si contente effects on compressive strengths of Al/Si/Cu composites. Mater Sci Eng A 770 (2020) 13847.
18. Bonatti RS, Siqueira RR, Padilha GS, Bortolozo AD, Osório WR. Distinct Alp/Sip composites affecting its densification and mechanical behavior. J Alloys Compd 757 (2018) 434-447.
19. Meyer YA, Bonatti RS, Costa D, Bortolozo AD, Osório WR. Compaction pressure and Si contente effects in compressive strengths of Al/Si/Cu alloy composites. Mater Sci Eng A 770 (2020) 13847.
20. Fogagnolo JB, Robert MH, Torralba JM. Mechanically alloyed AlN particle-reinforced Al-6061 matrix composites: Powder processing, consolidation and mechanical strength and hardness of the as-extruded materials. Mater Sci Eng A 426 (2006) 85-94.

21. Espinosa-Méndez C, Maquieira CP, Arias JT. The impact of ESG performance on the value of family firms: The moderating role of financial constrainsts and agency problems. Sustainab 15 (2023) 6176.
22. Kurz W, Fisher DJ, Fundamentals of Solidification, Trans. Tech. Public, Switzerland, 1992.
23. Hamza HM, Deen KM, Haider W. Microstructural examination and corrosion behavior of selective laser melted and conventionally manufactured Ti6Al4V for dental applications. Mater Sci Eng C 113 (2020) 110980.
24. The Materials Project, accessed from https://next-gen.materialsproject.org, Al2Cu/mp-998.
25. Alam SN, Shrivastava P, Panda D, Gunale B, Susmitha K, Pola P. Synthesis of Al2Cu intermetallic compound by mechanical alloying.Mater Today Communications 31 (2022) 103267.
26. Zhou J and Duszczyk J. Preparation of Al-20Si-4.5Cu alloy and its composite from elemental powders. J Mater Sci 1999; 34: 5067–5073.
27. Ramberger R, Burger A. On the application of the Heckel and Kawakita equation to powder compaction. Powder Technol 43 (1985) 1-9.
28. Han P, An ZH, Wang D, Fu H, Yang XH, Zhang H, Zou Z. MPFEM simulation of compaction densification behavior of Fe-Al composite powders with different size ratios. J Alloys Compds 741 (2018) 473-481.
29. Bonatti RS, Meyer YA, Bortolozo AD, Costa D, Osório WR. Morphology and size effects on densification and mechanical behavior of sintered powders from Al-Si and Al-Cu casting alloys. J Alloys Compds 786 (2019) 717-732.
30. Bouvard D. Densification behaviour of mixtures of hard and soft powders under pressure. Powder Technol. 111 (2000) 231–239.
31. Hafizpour HR, Simchi A. Investigation on compressibility of Al–SiC composite powders. Powder Metall. 51 (2008) 217–223.
32. Gokçe A, Findik F. Mechancial and physical properties of sintered aluminum powders. J Achiev Mater Manufact Eng 30 (2008) 157-164.
33. Sweet GA, Brochu M, Hexemer Jr RL, Donaldson IW, Bishop DP. Microstructure and mechanical properties of air atomized aluminum powder consolidated via spark plasma sintering. Mater Scie Eng A 608 (2014) 273-282.
34. Jonsén P, Haggblad HA, Sommer K. Tensile strength and fracture energy of pressed metal powder by diametral compression test. Powder Technol. 176 (2007) 148-155.
35. Procopio At, Zavaliangos A, Cunningham JC. Analysis of the diametrical compression test and the applicability to plastically deforming materials. J Mater Sci 38 (2003) 3629-3639.
36. Aguechari N, Boudiaf A, Ouali MO. Effect of artificial aging treatment on microstructure, mechanical properties and fracture behavior of 2017A alloy. Metall Mater Eng 28 (2022) 305-318. doi.org/10.30544/744.
37. Vargas-Martínez J, Estela-García, Suárez OM, Vega CA. Fabrication of a porous metal via selective phase dissolution in Al-Cu alloys. Metals 8 (2018) 378-396. doi:10.3390/met8060378.
38. Zhang Y, Li R, Chen P, Li X, Liu Z. Microstructural evolution of Al2Cu phase and mechanical properties of the large-scale Al alloy components under different consecutive manufacturing processes. J Alloys Compds 808 (2019) 151634.